# THE STRUCTURE AND SPECTROSCOPY OF $Gd_2Y_{(1-x)}Ce_xAl_2Ga_3O_{12}$ PHOSPHOR FOR X-RAY DETECTION MATERIAL

**Eakgapon Kaewnuam[1,*], Anon Angnanon[2,3], Fueangfa Khrongchaiyaphum[2,3], Ladawan Chotirat[1], Worakan Sukwanichwichai[1], Nuanthip Wantana[2,3] and Jakrapong Kaewkhao[2,3]**

*Received: December 29, 2023; Revised: February 19, 2024; Accepted: March 06, 2024*

## Abstract

**This work aimed to synthesis and study the $Gd_2Y_{(1-x)}Ce_xAl_2Ga_3O_{12}$ phosphor for radiation detection applications. The influence of Ce content on structural, optical and luminescence properties of phosphor were analyzed. Phosphor samples were prepared by the solid-state reaction. The XRD results presented the cubic crystalline structure in $Ia\bar{3}d$ space group. Phosphors absorbed the photons in ultraviolet and visible light region by $Ce^{3+}$, $Gd^{3+}$ and host component. The ultraviolet excitation with 444 nm (direct $Ce^{3+}$ excitation) and 275 nm (energy transfer from $Gd^{3+}$) generated the strong photoluminescence at 518 and 469 nm. The emission from another discrete energy levels were found and enhanced the photoluminescence of some samples. The X-rays induced luminescence spectra performed the obvious emission from $Ce^{3+}$ that phosphor with Ce content as 0.09 owned the highest intensity. Due to the strong luminescence and short decay time around 19 ns, the $Gd_2Y_{0.91}Ce_{0.09}Al_2Ga_3O_{12}$ phosphor has potential for the X-ray imaging screen and detectors.**

**Keywords: Phosphor; Luminescence; Cerium; Gadolinium**

## Introduction

The luminescence powder as known as phosphor have been widely used in the light / photon related devices. It can apply in the display, fluorescence lamp, light emitting diode (LED), watch, medical imaging screen, flaw detection and security inspection. The phosphor for radiation-detecting usage requires the high radiation absorption coefficient, suitable band gap, efficient energy transfer to luminescence center and high light output. There are the interesting compounds in family of multi-components $(Gd,Y)_3(Al,Ga)_5O_{12}$ garnets which have been studied and developed as the single-crystal (Ashurov *et al*., 1977; Kamada, *et al*., 2011; Chewpraditkul *et al*., 2017), ceramic

[1] *Physics Program, Faculty of Science and Technology, Muban Chombueng Rajabhat University, Ratchaburi, 70150, Thailand. E-mail: Eakgapon_9@hotmail.com*
[2] *Physics Program, Faculty of Science and Technology, Nakhon Pathom Rajabhat University, Nakhon Pathom, 73000, Thailand.*
[3] *Center of Excellence in Glass Technology and Materials Science (CEGM), Nakhon Pathom Rajabhat University, Nakhon Pathom, 73000, Thailand*
[*] *Corresponding author*

*DOI: https://doi.org/10.55766/sujst-2024-02-e03146*

**Suranaree J. Sci. Technol. 31(2):030173(1-7)**

(Chen *et al*., 2020) and phosphor (Asami *et al*., 2018; Kaura *et al*., 2020; Ou *et al*., 2020) for radiation detection materials. The enhancement of host band gap by using optimal ratio between Gd and Ga content can bury the shallow traps and degrade the thermal ionization of luminescence $Ce^{3+}$ dopant. The $Gd^{3+}$ with large effective atomic number in this garnet supports the efficient interaction with incoming photons, and sequentially transfers the excitation energy to the luminescence dopant. From these properties, it caused the high light yield, small energy resolution and fast decay time in $Gd_2YAl_2Ga_3O_{12}:Ce^{3+}$ garnet single crystal [1]. The $Ce^{3+}$ has the signature 4f-5d transitions generating the strong and board emission in ultraviolet (UV) - visible light (VIS) with short decay time. It also quite responds to the photo-multiplier tube (PMT) integrated in the commercial radiation detector. Since the 5d orbital of $Ce^{3+}$ is not shelled by 5s and 5p like 4f one, the 5d states are normally disturbed by the crystal field and coordination nature with surround atoms/ions. This causes the fluctuation of 5d states and the shift of emission peak based on the $Ce^{3+}$ location site in lattice (Ueda and Tanabe, 2019). Several $Ce^{3+}$-doped phosphors such as $BaF_2 : Ce^{3+}$ (Gavhane *et al*., 2019), $CaSc_2 O_4 : Ce^{3+}$ (Kang *et al*., 2019), $BaB_4O_7:Ce^{3+}$ (Gavhane *et al*., 2020), $Li_2Ca_2Si_2O_7:Ce^{3+}$ (Wu *et al*., 2020), and $Gd_2YAl_2Ga_3O_{12}:Ce^{3+}$ (Asami *et al*., 2018) have been studied and developed for the radiation detection devices. The last one gave the attractive luminescence under suitable energy gap between conduction band (CB) and $5d_1$ state of $Ce^{3+}$ due to the optimal Gd/Ga ratio, previously mentioned. However, the optimum content of Ce dopant in this phosphor has never been investigated. Since the effective ionic radius of $Ce^{3+}$ ion (1.01 Å) is closed to one of $Y^{3+}$ ion (0.90 Å) (Ziolkowski, 1985), it is very interesting to study by replacing Y with Ce in phosphor structure. The effect of substitution should be studied from low to large content.

## Materials and Methods

The $Gd_2Y_{(1-x)}Ce_xAl_2Ga_3O_{12}$ phosphors were prepared by a solid state reaction. The x is Ce content of 0.00, 0.03, 0.09, 0.25, 0.50, 0.75 and 1.00 which was substituted on Y in composition. The label of sample is then Ce0.00, Ce0.03, Ce0.06, Ce0.09, Ce 0.12, Ce0.25, Ce0.50, Ce0.75 and Ce1.00, respectively. The high purity raw chemicals of $Gd_2O_3$, $Y_2O_3$, $CeF_3$, $Al_2O_3$ and $Ga_2O_3$ in stoichiometry were mixed with acetone and taken the ball-milling with 200 rpm for 2 h. Then, the powder was compressed to be the tablets by hydraulic press with 50 MPa. The tablets were calcined at 1000°C for 60 h and taken out to mash as a powder. After that, the calcined powder was pressed by hydraulic system to be the tablets again and were sintered at 1600°C for 10 h. The phosphors were left to cool down to room temperature.

The crystalline structure of phosphor was investigated by X-ray diffractometer (Shimadzu, XRD-6100) using the $CuK_\alpha$ radiation with wavelength of 1.54 Å. The absorption spectra in UV and VIS region of samples were monitored by UV-VIS-NIR Spectrophotometer (Shimadzu, UV-3600). The photoluminescence (PL) emission and excitation spectra of phosphors were studied by Fluorescence spectrophoto-meter (Hitachi, F-4600). The PL decay profiles were measured via the fluorescence lifetime measuring device (DD-290, Horiba Scientific) with 290 nm diode laser excitation. The radiation detection potential of phosphor was investigated by the radioluminescence (RL) spectra measurement. The RL experiment setup composes of the Cu target X-ray generator (Inel, XRG3D-E) operated by 50 kV and 30 mA power, the optical fiber - spectrometer (Ocean Optics, QE65 Pro) and the cooling system.

## Results and Discussion

The prepared $Gd_2Y_{(1-x)}Ce_xAl_2Ga_3O_{12}$ phosphor samples with cylindrical shape (diameter = 2 cm, height = 1 cm) are represented in Figure 1. The color of undoped Ce0.00 phosphor is white, while the rest samples with $Ce^{3+}$ dopant own yellow color.

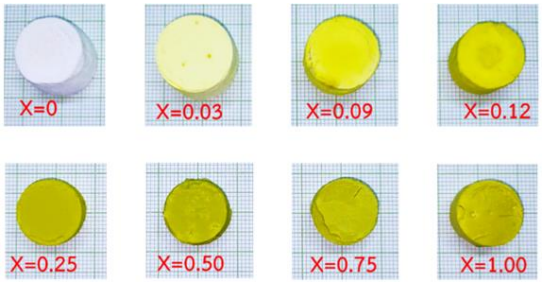


**Figure 1. $Gd_2Y_{(1-x)}Ce_xAl_2Ga_3O_{12}$ phosphor samples**

### Crystalline structure

The pattern of X-ray diffraction (XRD) for all phosphors are represented in Figure 2(a). The $Gd_2YAl_2Ga_3O_{12}$ (Ce0.00) phosphor owned the pattern corresponding to the database of $Gd_3Al_3Ga_2O_{12}$ crystalline garnet (JCPDS 00-046-0448). It is the cubic structure with $Ia\bar{3}d$ space

group, typical $\{A\}_3[B]_2(C)_3O_{12}$ garnet structure. The main diffraction peak belonged to (4 2 0) atomic plane. The dodecahedral {A} site is occupied by $Gd^{3+}$ or $Y^{3+}$ ion. The octahedral [B] and tetrahedral (C) site can be occupied by both $Al^{3+}$ or $Ga^{3+}$ ion (Uemura *et al.*, 2008; Ueda and Tanabe, 2019). Furthermore, the strength of garnet peaks decreased that exhibited more structural perturbation via adding Ce content.

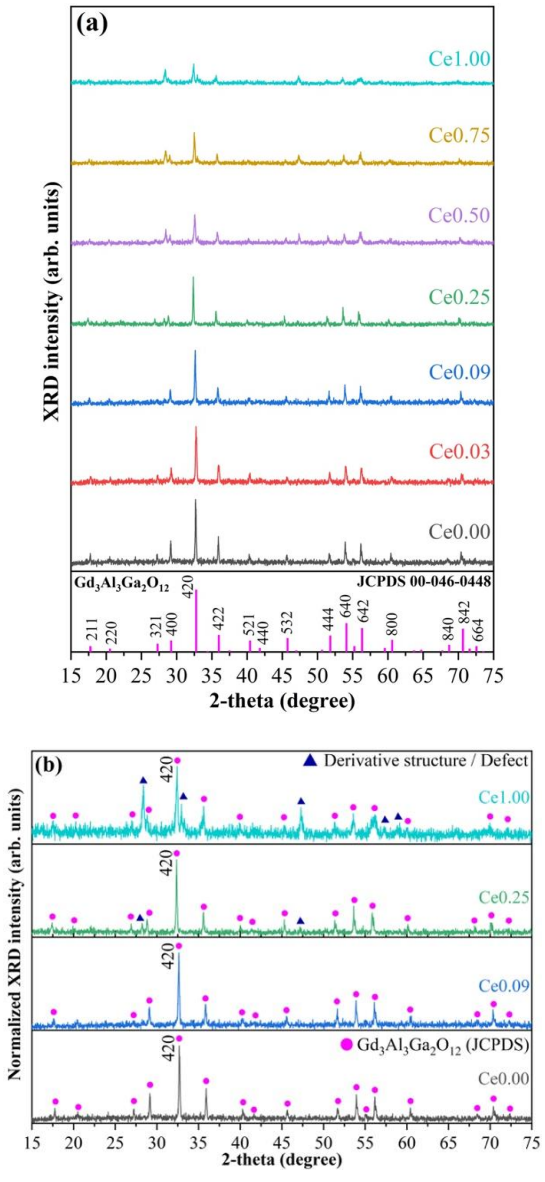


**Figure 2. (a) XRD pattern of $Gd_2Y_{(1-x)}Ce_xAl_2Ga_3O_{12}$ phosphors compared with the JCPDS data base (b) Normalized XRD pattern of Ce0.00, Ce0.09, Ce0.25 and Ce1.00 phosphor**

The comparative XRD in normalized scale of some phosphors are shown in Figure 2(b) with markers of diffraction peaks. The diffraction pattern of phosphor with $x \leq 0.09$ still conserved as same as Ce0.00, while ones with $x \geq 0.25$ had the additional diffraction peaks. Those additional peaks possibly related to the formation of derivative structures around the micro grains, and defects. Since $Gd^{3+}$, $Y^{3+}$ and $Ce^{3+}$ have close ionic radius (1.05, 0.90 and 1.01 Å, respectively), the added $Ce^{3+}$ ion could locate at $Y^{3+}$ and $Gd^{3+}$ position in {A} site. The additional diffraction peaks did not appear in phosphor with low Ce content ($x \leq 0.09$) representing the accomplished replacement of Y by Ce in original garnet structure. However, the ionic radius of $Ce^{3+}$ is slightly larger than $Y^{3+}$ which caused some uncomplete Y-Ce substitution in high Ce content ($x \geq 0.25$). Then, there were such derivative structures and defects existing in phosphor. The main diffraction peak with (h k l) = (4 2 0) was chosen to analyze the details of phosphor lattice as shown in Figure 3.

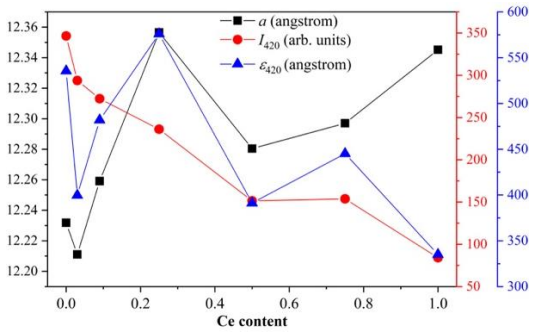


**Figure 3. (a) The lattice constant ($a$), XRD intensity for (4 2 0) plane ($I_{420}$) and crystallite size of (4 2 0) plane ($\varepsilon_{420}$) in $Gd_2Y_{(1-x)}Ce_xAl_2Ga_3O_{12}$ phosphors with different Ce content**

The lattice constant ($a$) represents the shortest distance between atom/ion at the cubic lattice's corner. From calculating via Bragg's law and spacing formula (Warren, 1990), $a$ value slightly dropped in Ce0.03 compared to Ce0.00 sample. For $0.03 \leq x \leq 0.25$, it increased with Ce addition and changed to oscillate in phosphors with $x \geq 0.25$. The minimum and maximum $a$ value of phosphor was 12.21 Å (Ce0.03) and 12.36 Å (Ce0.25) those was corresponding to 12.21 Å of $Gd_3Al_3Ga_2O_{12}$ data base. The XRD intensity ($I_{420}$), exhibiting the degree of atomic ordering for (4 2 0) plane, tended to

decrease with Ce increment. For the crystallite size ($\varepsilon_{420}$) calculated via Scherrer's Equation (Langford and Wilson, 1978), it decreased, increased, and roughly decreased with Ce addition in range of $0.00 \le x \le 0.03$, $0.03 \le x \le 0.25$ and $0.25 \le x \le 1.00$, respectively. The $\varepsilon_{420}$ value relates inversely to the crystallite boundary. Ce1.00 phosphor with small $\varepsilon_{420}$ value (335.10 Å) owned a lot of crystallite boundary, while Ce0.25 phosphor with large $\varepsilon_{420}$ (575.87 Å) had less boundary. From considering overall XRD results, the Y→Ce replacement by x = 0.03 caused $Ce^{3+}$ acting as the impurity in crystalline system. The value of *a*, $I_{420}$ and $\varepsilon_{420}$ then reduced in Ce0.03 compared to Ce0.00 sample. For $0.03 \le x \le 0.25$, the Y substitution by Ce also degraded the crystalline quality that's why $I_{420}$ continuously decreased but the lattice still conserved as the original garnet structure. Since enough Ce amount that the lattice was not considered $Ce^{3+}$ as an impurity anymore and this ion could locate quite in dodecahedral {A} site, $\varepsilon_{420}$ increased in this range of Ce content. The *a* value also increased in this Ce range because the ionic radius of $Ce^{3+}$ is slightly larger than $Y^{3+}$. Phosphor with x = 0.25 was the last stand that could keep the single phase of original garnet with maximum distortion. In the range of $0.25 \le x \le 1.00$, $I_{420}$ and $\varepsilon_{420}$ decreased while *a* oscillated due to the structure degradation by existence of derivative structure / defect.

The structure of phosphor can affect to its luminescence properties. The long lattice constant help to prevent the Ce-Ce interaction that causes the concentration quenching. The large crystallite size with less crystallite boundary leads to the low probability of photon scattering. The degraded quality of lattice can fluctuate the luminescence intensity and decay time.

**Absorption Spectra**

The absorption spectra of phosphors in UV-VIS region are represented in Figure 4(a). The absorption spectrum of host Ce0.00 sample is presented as dash line that its tail reached almost 400 nm. There was an absorption peak of $Gd^{3+}$ ion under the $^8S_{7/2} \rightarrow {}^6I_{17/2}$ transition (275 nm) in the absorption edge region. For phosphors with Ce, there were the additional absorption peaks under 4f→5d transitions those were overlapped in that region. The absorption spectra could be separated into two regions. The first one was the superposed absorption between $Ce^{3+}$, $Gd^{3+}$ and the other phosphor composition in a range of 200 - 390 nm. The second one between 390 - 520 nm belonged to only $Ce^{3+}$ ion which the Ce0.09 phosphor performed the strongest absorbance relatively to its absorption maximum in the first region. The measured absorption spectrum of Ce0.09 and Ce0.00 phosphor was presented in Figure 4(b). The absorbance of Ce0.00 host was dense in UV region with tail reaching almost 400 nm, while one of Ce0.09 distributed in UV and VIS region before 530 nm. It can be said that the existence of Ce dopant perturbed the absorption transition of host component to be less in UV region and spread out into VIS region via mixing with $Ce^{3+}$ transition.

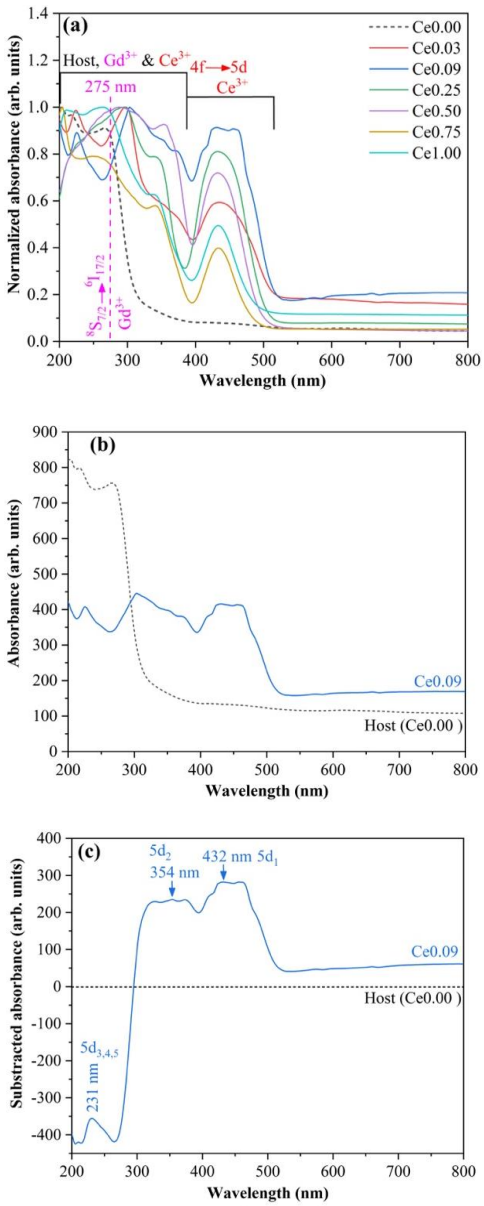


**Figure 4. (a) Normalized absorption spectra of $Gd_2Y_{(1-x)}Ce_xAl_2Ga_3O_{12}$ phosphors, (b) Comparative spectrum of Ce0.09 and Ce0.00 sample and (c) Absorption spectrum of Ce0.09 sample subtracted with one of Ce0.00**

The absorption spectrum of Ce0.09 sample was subtracted by one of host and shown in Figure 4(c). The pure absorption transitions of $Ce^{3+}$ then were obvious in three groups. The 4f →$5d_1$, 4f →$5d_2$ and 4f →$5d_{3,4,5}$ transitions absorbed maximally the photons around 432, 354 and 231 nm respectively. Since the last one was lower than the subtracted absorption of host, the energy level of 4f →$5d_{3,4,5}$ transition possibly superposed in the host's valence band. Furthermore, the 4f →5d transitions of $Ce^{3+}$ occupied in wide absorption range. The crystal field perturbation from $Ce^{3+}$ site caused its wide distribution of 5d-band energy level.

**Photoluminescence spectra**

The PL spectra with emission wavelength ($\lambda_{EM}$) at 518 nm and excitation wavelength ($\lambda_{EX}$) at 444 nm were represented in Figure 5(a). For emission spectra under $\lambda_{EX}$ = 444 nm, the electrons in $Ce^{3+}$ was raised from 4f state to excited $5d_1$ orbital and then non-radiatively relaxed to the lowest vibrational state of $5d_1$. After that, the $5d_1$→4f transition of $Ce^{3+}$ generated the broad emission between 480 – 650 nm (center at 518 nm for Ce0.25 phosphor) (Asami *et al*., 2018; Tian *et al*., 2022). This emission of $Ce^{3+}$ in Ce0.09 and Ce0.25 phosphor was huge due to the superposition with additional luminescence centering at 480 nm from unidentified discrete energy (UDE). This UDE was probably the interstitial states created by the overlap of 5d orbital and valence band of host in phosphor with optimum Ce content such as x = 0.09 and 0.25. For phosphor with other Ce amount, such luminescence was disappeared. In the excitation spectra with $\lambda_{EM}$ = 518 nm, there were the peaks at 350 and 444 nm under the excitation transitions of $Ce^{3+}$, 4f→$5d_2$ and 4f→$5d_1$, respectively. Both transitions in Ce0.09 and Ce0.25 were boosted up by overlapping with transition from UDE. The existence of peak center around 480 nm in both emission and excitation spectra could be evident the energy transfer between UDE and $Ce^{3+}$ in phosphor. Furthermore, there were the possibility that $\lambda_{EX}$ = 444 nm could also excite to UDE and make itself luminescence. The highest PL intensity at $\lambda_{EM}$ = 518 nm of Ce0.25 sample was possibly dependent by concentration quenching (less Ce-Ce interaction by long lattice constant and low Ce amount), low photon scattering by less crystallite boundary (large crystallite size) and supporting from UDE. The PL emission spectra under $\lambda_{EX}$ = 275 nm are represented in Figure 5(a). This UV excitation provided the $^8S_{7/2}$→$^6I_{17/2}$ transition of $Gd^{3+}$ before this ion non-radiatively relaxed to $^6P_{7/2}$ state. At this point, some $Gd^{3+}$ could transfer the energy to $Ce^{3+}$ (Kaewnuam *et al*., 2022) and some probably transferred the energy to UDE. The $Ce^{3+}$ acceptor then non-radiatively relaxed to the lowest vibrational state of 5d orbital before it emitted the photons via $5d_2$→ 4f transition at 359 nm, and probably also $5d_1$→4f transition but could not determine its wavelength due to the superposition with UDE emission. For UDE acceptor, it consequently generated the broad and huge emission covering 325 - 650 nm with spike peaks around 469 nm, especially in Ce0.09 and Ce0.25 sample. It also cannot refuse that $\lambda_{EX}$ = 275 nm possibly excited UDE and made its direct luminescence. The highest PL intensity at $\lambda_{EM}$ = 359 and 469 nm of Ce0.09 phosphor were based-on the concentration quenching (less Ce-Ce interaction by low Ce amount) and entanglement with UDE.

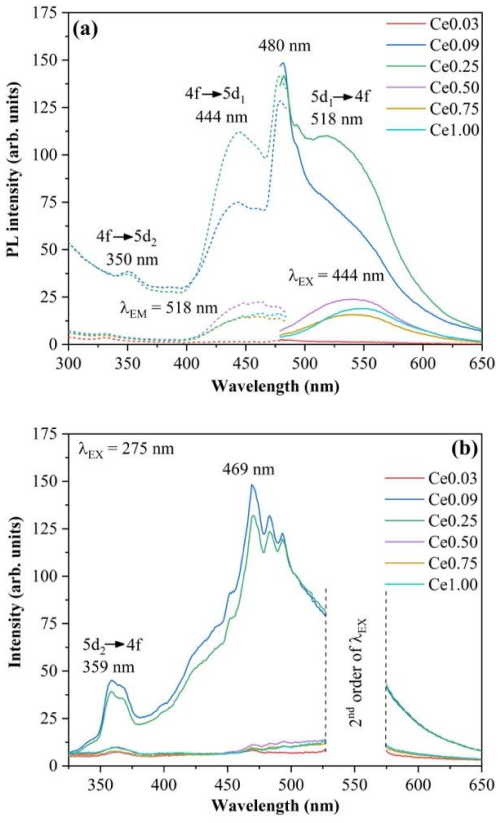


**Figure 5. (a) PL emission spectra with $\lambda_{EX}$ = 444 nm (solid line), excitation spectra with $\lambda_{EM}$ = 518 nm (dash line) and (b) PL emission spectra with $\lambda_{EX}$ = 275 nm of $Gd_2Y_{(1-x)}Ce_xAl_2Ga_3O_{12}$ phosphors**

**Photoluminescence Decay**

Figure 6 presented the PL decay profiles under $\lambda_{EX}$ = 290 nm of phosphors. The overall behavior of curves corresponded to the single exponential decay then they were fitted with this expression. The obtained decay time (τ) decreased with rising of Ce content with 0.03 ≤ x ≤ 0.75 due to the concentration

quenching (Ce-Ce interaction with more Ce content) and turned to increase at x = 1.00 probably due to the fluctuation by degraded quality in crystalline structure. The τ values were between 13.66 - 20.51 ns those were short and good response for using this phosphor in the radiation detecting applications.

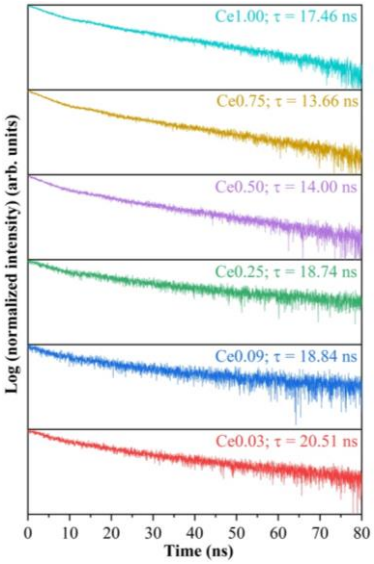


**Figure 6. PL decay curves of $Gd_2Y_{(1-x)}Ce_xAl_2Ga_3O_{12}$ phosphors**

**Radioluminescence spectra**

The RL is very significant to indicate the potential of radiation detection material. In Figure 7, the RL emission peak between 450 - 800 nm centering at 554 nm looks Gaussian and there was not any spike peak. Therefore, the main source of RL came from $5d_1 \rightarrow 4f$ transition of $Ce^{3+}$ ion. The incoming X-ray were absorbed by host components in phosphor and generated the electron - hole pairs by photoelectric effect and Compton scattering. The electron and hole then moved in the conduction and valence band, respectively and ready for the recombination. Finally, that electron-hole pair moved to combine at the discrete energy levels and provided the luminescence (Nikl, 2006). Some electron - hole pairs recombined at the inter 5d-4f level of $Ce^{3+}$ ion and some at intra 4f-4f orbital of $Gd^{3+}$. The $Ce^{3+}$ ion then generated the emission by itself and by receiving the energy transferred from $Gd^{3+}$. The RL intensity increased with adding Ce content in $0.03 \leq x \leq 0.09$ and decreased in range of $0.09 \leq x \leq 1.00$ due to the concentration quenching effect. Contrast to PL, the influence of structure and UDE were not obvious on the RL spectra. The X-ray possibly created the damage or disturbed on phosphor structure which relegated the effect of structure on RL property. The Ce0.09 performed the highest RL intensity similarly to PL with $\lambda_{EX}$ = 275 nm, revealing the influence of Gd→Ce energy transfer on X-ray detection. Furthermore, the most of its RL peak located by overlapping with RL of bismuth germanium oxide (BGO) single crystal. These results exhibited the high potential for using $Gd_2Y_{0.91}Ce_{0.09}Al_2\ Ga_3O_{12}$ as the X-ray detection material.

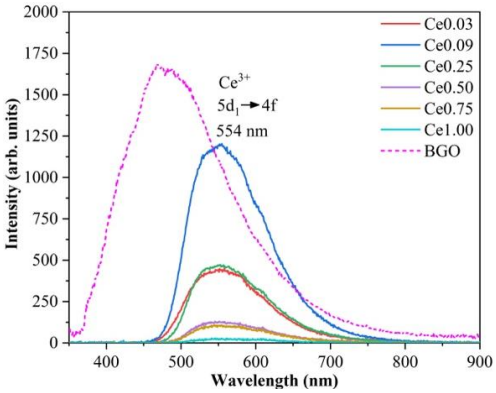


**Figure 7. RL spectra of $Gd_2Y_{(1-x)}Ce_xAl_2\ Ga_3O_{12}$ phosphors under X-ray induction (solid line) compared to BGO crystal (dash line)**

## Conclusions

The series of $Gd_2Y_{(1-x)}Ce_xAl_2Ga_3O_{12}$ phosphors, synthesized by solid state reaction, owned the cubic crystalline structure in Ia $\bar{3}$ d space group. The derivative structures and defects appeared in phosphor with Ce content in a range of 0.25 - 1.00. The lattice constant increased with added Ce content from 0.03 - 0.25 and oscillated for Ce amount over than 0.25 due to modified structures. The (4 2 0) diffraction intensity tended to decrease revealing the structure degradation via Ce addition. The crystallite size of (4 2 0) plane fluctuated by varying the Ce content that the Ce0.25 and Ce1.00 phosphor possessed the highest and lowest one, respectively. The phosphors absorbed photon in UV and VIS region by $Ce^{3+}$, $Gd^{3+}$ and host component. The UV excitation with 444 and 275 nm generated the PL emission of $Ce^{3+}$ by direct excitation and the Gd→Ce energy transfer, respectively. However, the PL of phosphor were entangled with UDE which boosted up the PL intensity in Ce0.09 and Ce0.25 phosphor. The other effect factors for PL intensity were concentration quenching and crystallite boundary. However, the RL intensity under X-ray excitation was influenced by concentration

quenching only that Ce0.09 owned the strongest emission. The PL decay time decreased by concentration quenching, except Ce1.00 that it increased possibly due to the perturbation of degraded structure. From strong PL / RL and short decay time around 19 ns, the $Gd_2Y_{0.91}Ce_{0.09}Al_2Ga_3O_{12}$ phosphor in this work performed the high potential for X-ray detection applications such as in X-ray imaging screen and detectors.

## Acknowledgement

This work has been funded by Thailand Science Research and Innovation (TSRI) in project No.50165 (2021). The authors so appreciate with Muban Chombueng Rajabhat University and Center of Excellence in Glass Technology and Materials Science (CEGM) - Nakhon Pathom Rajabhat University for facilities in this research.

## References

Asami, K., Ueda, J., Kitaura, M., and Tanabe, S. (2018). Investigation of luminescence quenching and persistent luminescence in $Ce^{3+}$ doped $(Gd,Y)_3(Al,Ga)_5O_{12}$ garnet using vacuum referred binding energy diagram. Journal of Luminescence, 198:418-426. https://doi.org/10.1016/j.jlumin.2018.01.041

Ashurov, M.Kh., Voronko, Yu.K., Osiko, V.V., Sobol, A.A., and Timoshechkin, M.I. (1977). Spectroscopic Study of Stoichiometry Deviation in Crystals with Garnet Structure. Physica Status Solidi (a), 42(1):101-110. https://doi.org/10.1002/pssa.2210420108

Chen, X., Liu, X., Feng, Y., Li, X., Chen, H., Xie, T., Kou, H., Kucerkova, R., Beitlerova, A., Mihokova, E., Nikl, M., and Li, J. (2020). Microstructure evolution in two-step-sintering process toward transparent $Ce:(Y,Gd)_3(Ga,Al)_5O_{12}$ scintillation ceramics. Journal of Alloys and Compounds, 846:1-16. https://doi.org/10.1016/j.jallcom.2020.156377

Chewpraditkul, W., Sakthong, O., Pattanaboonmee,N., Chewpraditkul,W., Szczesniak, T., Swiderski, L., Moszynski, M., Kamada, K., Yoshikawa, A., and Nikl, M. (2017). Optical and scintillation characteristics of $Gd_2YAl_2Ga_3O_{12}$:Ce and $Lu_2YAl_2Ga_3O_{12}$:Ce single crystals. Journal of Crystal Growth, 468:395-398. https://doi.org/10.1016/j.jcrysgro.2016.10.086

Gavhane, K.H., Bhadane, M.S., Bhoir, A.S., Kulkarni, P.P., Dahiwale, S.S., Patil, B.J., Bhoraskar, V.N., and Dhole, S.D. (2020). $T_m$-$T_{stop}$ analysis and dosimetric properties of Ce doped $BaB_4O_7$ phosphor. Journal of Alloys and Compounds, 817:1-7. https://doi.org/10.1016/j.jallcom.2019.152805

Gavhane, K.H., Bhadane, M.S., Jadhav, A.P., Patil, B.J., Bhoraskar, V.N., Dahiwale, S.S., and Dhole, S.D. (2019). TL properties of $BaF_2$:Ce phosphor for high gamma ray dosimetry. Journal of Luminescence, 209:316-320. https://doi.org/10.1016/j.jlumin.2019.02.011

Kaewnuam, E., Wantana, N., Ruangtaweep, Y., Cadatal-Raduban, M., Yamanoi, K., Kim, H.J., Kidkhunthod, P., and Kaewkhao, J. (2022). The influence of $CeF_3$ on radiation hardness and luminescence properties of $Gd_2O_3$–$B_2O_3$ glass scintillator. Scientific Reports, 12:1-13. https://doi.org/10.1038/s41598-022-14833-3

Kamada, K., Yanagida, T., Pejchal, J., Nikl, M., Endo, T., Tsutumi, K., Fujimoto, Y., Fukabori, A., and Yoshikawa, A. (2011). Scintillator-oriented combinatorial search in Ce-doped $(Y,Gd)_3(Ga,Al)_5O_{12}$ multicomponent garnet compounds. Journal of Physics D: Applied Physics, 44:1-8. https://doi.org/10.1088/00223727/44/50/505104

Kang, T., Lim, S., Lee, S., Kang, H., Yu, Y., and Kim, J. (2019). Luminescent properties of $CaSc_2O_4$:$Ce^{3+}$ green phosphor for white LED and its optical simulation. Optical Materials, 98:1-5. https://doi.org/10.1016/j.optmat.2019.109501

Kaura, J., Rania, S., and Lal, B. (2020). Luminescence properties of $Eu^{3+}$ doped gadolinium aluminum garnet phosphors. Optik - International Journal for Light and Electron Optics, 212:1-5. https://doi.org/10.1016/j.ijleo.2020.164745

Langford J.I. and Wilson, A.J.C. (1978). Scherrer after Sixty Years: A Survey and Some New Results in the Determination of Crystallite Size. Journal of Applied Crystallography, 11:102-113. https://doi.org/10.1107/S0021889878012844

Nikl, M. (2006). Scintillation detectors for x-rays. Measurement Science and Technology, 17(4):37-54. https://doi.org/10.1088/0957-0233/17/4/R01

Ou, Y., Zhou, W., Ma, F., Liu, Ch., Zhou, R., Su, F., Huang, Y., Dorenbos, P., and H. Liang, (2020). Luminescence tuning of $Ce^{3+}$, $Pr^{3+}$ activated (Y,Gd)AGG system by band gap engineering and energy transfer. Journal of Rare Earths, 38:514-522. https://doi.org/10.1016/j.jre.2020.01.001

Tian, Y., Chen, J., Yi, X., Jiang, R., Lin, H., Chen, L., and Zhou, Sh. (2022). Unravel the effect of lattice distortion on the 4f-5d excitation of $Ce^{3+}$ in garnet phosphors. Journal of Alloys and Compounds, 907:1-7. https://doi.org/10.1016/j.jallcom.2022.164412

Ueda, J., and Tanabe, S. (2019). Review of luminescent properties of $Ce^{3+}$-doped garnet phosphors: New insight into the effect of crystal and electronic structure. Optical Materials: X, 1:1-19. https://doi.org/10.1016/j.omx.2019.100018

Uemura, M., Yamagishi, T., Ebisu, S., Chikazawa S., and Nagata, S. (2008). A double peak of the coercive force near the compensation temperature in the rare earth iron garnets. Philosophical Magazine, 88(2):209-228. https://doi.org/10.1080/14786430701805582

Warren, B.E. (1990). X-RAY DIFFRACTION. Dover Publications, Inc., NY, 389p.

Wu, Q., He, Z., Huang, Q., Zhao, Q., Zheng, P., Xiang, D., Ding, J., and Zhou, J. (2020). The electronic structure, site occupancy and luminescent properties of $Ce^{3+}$-activated $Li_2Ca_2Si_2O_7$ blue phosphor. Ceramics International, 46(4):4511-4518. https://doi.org/10.1016/j.ceramint.2019.10.178

Ziolkowski, J. (1985). New Relation between Ionic Radii, Bond Length, and Bond Strength. Journal of Solid State Chemistry, 57:269-290. https://doi.org/10.1016/0022-4596(85)90152-5